Real-time Identification of High-Lift Devices Deployment in Aircraft Descents

An Interacting Multiple Model Filtering Application Validated with Simulated Trajectories

Homeyra Khaledian, Xavier Prats
Dept. of Physics/Aeronautics Division
Technical University of Catalonia UPC/BarcelonaTECH
Castelldefels, Spain
homeyra.khaledian@upc.edu
xavier.prats@upc.edu

Jordi Vilà-Valls
Institut Supérieur de l'Aéronautique et de l'Espace
(ISAE-SUPAERO)
University of Toulouse
Toulouse, France
jordi.vila-valls@isae-supaero.fr

***Abstract*—In this contribution, we focus on the real-time identification of the moment high-lift devices (typically flaps and slats) are deployed, based on surveillance input data. This estimation aims to enhance ground-based trajectory predictors (TP), that might equip a wide range of tools or systems: from air traffic control decision support tools, to ground-based safety nets, including alerting/monitoring systems in charge to detect atypical flight conditions. Given the fact that aircraft fly according to different guidance modes, a multiple model filtering strategy is proposed to cope with such different system dynamics. The filter provides a model probability associated with each guidance mode, which in turn can be exploited to obtain an estimate of the high-lift deployment moment. The proposed methodology is validated with a set of simulated realistic trajectories, showing good performance and promising capabilities.**

***Keywords*—Air traffic management, flight execution phase trajectory prediction, high-lift device deployment, IMM filtering.**

I. Introduction

Maintaining the highest safety level in aviation has always been a big challenge especially in the context of the rapidly increasing air traffic which is projected to reach 7.8 billion passengers in 2036 Such growth will require innovative decision support tools which will enable the increase in capacity, predictability and eventually enhancing the safety. Therefore, civil aviation authorities of large number of states worldwide deployed the national safety programs in order to be complied with the International Civil Aviation Organization (ICAO) safety requirements which define different categories of undesirable events, such as unstabilised approaches or control flight into terrain (CFIT) accidents [1].

The final stages of the approach procedure and landing represent every year the 47% of the total number of accidents, with the 40% of the total fatalities [2]. The majority of these accidents show unstabilised approaches, as consequence of atypical trajectory profiles in the vertical trajectory domain (speed and/or altitude), which in turn are sometimes the consequence of atypical trajectory profiles in the lateral trajectory domain (due, for instance, to turns to final too close to the runway).

According to [3], an approach is stabilized only if all the criteria in company standard operating procedures (SOPs) are met before or when reaching the applicable minimum stabilization height. Typically these criteria include a constant approach speed, a stable decent rate (vertical speed) within some margins, a stable descent flight path angle, the aircraft high-lift devices configured for landing, and the landing clearance received. These criteria shall typically be met at $1,000$ ft above the runway threshold in instrument meteorological conditions, or 500 ft in visual meteorological conditions. Otherwise, a go-around should be executed by the aircraft crew, since failing to achieve these stabilisation criteria, can seriously compromise the safety of the flight.

Many studies have been conducted to predict (hidden) flight parameters using surveillance data [1], [4]–[7]. To the best of our knowledge, few works specifically tackled the estimation of the moment high-lift devices are deployed. For instance, it is worth pointing out that a Long-Short Term Memory approach was used for real-time estimation of some aircraft on-board parameters (i.e., fuel flow rate, landing gear and flap configuration settings) in [4]. For this purpose, Flight Data Recorder (FDR) data was used to train a model and Aircraft Dependent Surveillance-Broadcast (ADS-B) data was used to feed a Neural Network structure. The average distance estimation error for different flap configurations was found to be between 2.27 NM to 0.88 NM [4].

In this paper we present a methodology to identify, in real-time, the moment that high-lift devices are deployed on descending aircraft trajectories, relying exclusively on surveillance data as input source. We focus exclusively to detect the moment the first high-lift configuration is deployed (i.e. the transition from what is typically called *clean* configuration, to the first high-lift configuration setting). Then, the goal is to resort to real-time filtering techniques in order to recursively estimate the aircraft states and high-lift devices deployment moment. A fundamentally different approach is proposed, where there is no need of training data, as it relies on model-based techniques.

This contribution could help to develop future ground-based

monitoring tools, aiming at detecting atypical trajectories and/or preventing unstabilised approaches. Moreover, it could as well enhance ground-based trajectory prediction algorithms that are enablers of a wide range of ATM applications: from air traffic control decision support tools (such as arrival managers); to ground-based safety nets or separation monitoring tools (such as Medium Term Conflict Detection systems).

II. Background

A. High-lift Devices

Aeroplanes are typically equipped with high-lift devices, which are designed to increase the maximum lift coefficient of the wing. This increase in maximum lift reduces the stall speed and therefore, allows the aircraft crew to fly the aircraft at lower speeds and, ultimately, reduce the take-off and landing distances. These devices also increase (significantly) the aerodynamic drag and consequently, are only and specifically used in the take-off and initial climb; and final stages of the approach and landing.

There are many types of such devices and the ones typically equipping modern airliners are the flaps (mounted in the trailing edge of the wing) and the slats (in the leading edge). Essentially, these devices increase the camber of the airfoil; and/or increase the wet surface of the wing (typically increasing the chord); and/or perform some control or effect on the boundary layer behaviour [8].

High-lift devices typically have different positions or configurations and are progressively deployed during the approach. Similarly, an aeroplane takes-off with a given high-lift device configuration and the crew progressively retracts them during the initial climb. The configuration where all high-lift devices are retracted is typically called *clean configuration*, and other configurations will receive different operational names depending on the aircraft type.

For example, for most Airbus models there are 5 different configurations CONF 1, CONF 1+F, CONF 2, CONF 3, and FULL. Take-offs are typically performed at CONF1+F or CONF2 and higher configurations are only used in very specific or exceptional situations, due to the high induced drag, which significantly degrades the climb performance. CONF1+F deploys (partially) slats and flaps. During an approach, CONF 1 is initially selected (which deploys partially slats) and then CONF 2 follows. Landings are typically performed in CONF 3 or FULL. Boeing aircraft, in turn, use a different nomenclature: for the B777 or B787, for instance, Flap 1 (only slats extended), Flaps 5 (slats and flaps), Flaps 15, Flaps 20... Yet, the operation is similar.

Each high-lift device configuration has a minimum and maximum speed where it can be operated and the pilots typically deploy/retract high-lift devices when reaching a certain speed and/or altitude, according to the aircraft SOP. Yet, the exact moment where they are deployed/retracted may vary even for the same aircraft model and same crew flying that aircraft. In fact, as long as these devices are operated within the speed minimum/maximum range, the crew can deploy/retract high-lift devices sooner or later. Many environment variables affect the exact moment the crew will use these devices, such as weather (especially in gusting wind conditions), obstacles below the flight path, actual climb/descent performance, but also, how *busy* is the crew in performing other tasks (i.e., communicating with air traffic control, executing more or less complex depart/approach procedures, interacting with the Flight Management Systems (FMS), etc).

As commented before, aerodynamic drag is increased when high-lift devices are used. Indeed, the drag coefficient is increased because of higher induced drag caused by the distorted span-wise lift distribution on the wing with flaps extended [8]. To a lesser extent, the parasite drag coefficient might also increase. Thus, aircraft performance models typically specify different drag coefficient parameters for each high-lift device configuration of the aircraft.

B. Aircraft descent guidance modes

FMS on-board modern aircraft employ automatic flight control systems to guide the aircraft along a previously computed trajectory (the reference trajectory or trajectory plan), and a series of flight guidance modes, both in the lateral path and in the vertical profile (altitude and speed). In general, there exist two classes of guidance modes to direct the aircraft: managed modes, which direct the aircraft along the reference trajectory as computed (and optimised) by the FMS; and selected (or open) modes, steering the aircraft according to manual inputs provided by the pilot (disconnected from the FMS trajectory plan).

FMS typically use a point-mass model representation of the aircraft dynamics, in which the aircraft motion is reduced to three degrees of freedom (the three translations), assuming that all forces are applied to the centre of gravity of the aircraft in equilibrium. Thus, vertical dynamics are subject to two degrees of freedom and there exist multiple vertical guidance modes, depending on which of the two of the three basic guidance targets are selected: airspeed (which can be in terms of Mach or calibrated airspeed (CAS)); altitude (which could be expressed in altitude-rate –i.e., vertical speed (VS)–, or flight path angle (FPA)) or fixed throttle setting. These guidance modes provide pitch (elevator) and thrust (throttle) commands and hence strongly interact with the auto throttle and autopilot systems. During cruise, the basic guidance target are straightforward (altitude and airspeed are held through a combination of elevator and throttle), but for climb and, particularly descent, multiple options are available, such as speed managed climb/descent, path managed descent, time-of-arrival-controlled climb/descent, etc. [7], [9].

This paper focuses to identify the exact moment the aircraft transitions from the clean high-lift devices configuration to the first configuration in an approach procedure. Therefore, the typical decent guidance modes have been taken into account and summarised in Table I. Modes keeping a constant Mach number are not considered, since these are typically used at high altitudes and speeds (where high-lift devices are not used). Similarly, acceleration modes have not been considered

TABLE I. DESCENT GUIDANCE MODES CONSIDERED IN THIS ARTICLE

Mode 1	Mode 2	Pilot input parameters	Control vector
Fixed Throttle (THR)	Deceleration (DEC)	$\mathbf{p}_k = [\pi = 0, e = k\|_{DEC}]$	$\mathbf{u}_{k-1} = [T = T_{idle}, \gamma = \arcsin(\frac{T_{idle} - D(\mathbf{x})}{mg})k\|_{DEC}]$
	Constant CAS (CAS)	$\mathbf{p}_k = [\pi = 0, e = k\|_{\dot{CAS}=0}]$	$\mathbf{u}_{k-1} = [T = T_{idle}, \gamma = \arcsin(\frac{T_{idle} - D(\mathbf{x})}{mg})k\|_{\dot{CAS}=0}]$
	Constant altitude (ALT)	$\mathbf{p}_k = [\pi = 0, VS = 0]$	$\mathbf{u}_{k-1} = [T = T_{idle}, \gamma = 0]$
Constant vertical speed (VS)	Deceleration (DEC)	$\mathbf{p}_k = [VS, e = k\|_{DEC}]$	$\mathbf{u}_{k-1} = [T = D(\mathbf{x}) + (\frac{mg}{k\|_{DEC}})(\frac{VS}{v}), \gamma = \arcsin(\frac{VS}{v})]$
	Constant CAS (CAS)	$\mathbf{p}_k = [VS, e = k\|_{\dot{CAS}=0}]$	$\mathbf{u}_{k-1} = [T = D(\mathbf{x}) + (\frac{mg}{k\|_{\dot{CAS}=0}})(\frac{VS}{v}), \gamma = \arcsin(\frac{VS}{v})]$
Constant flight path angle (FPA)	Deceleration (DEC)	$\mathbf{p}_k = [\gamma_g, e = k\|_{DEC}]$	$\mathbf{u}_{k-1} = [T = D(\mathbf{x}) + (\frac{mg}{k\|_{DEC}})\sin\gamma_g, \gamma = \gamma_g]$
	Constant CAS (CAS)	$\mathbf{p}_k = [\gamma_g, e = k\|_{\dot{CAS}=0}]$	$\mathbf{u}_{k-1} = [T = D(\mathbf{x}) + (\frac{mg}{k\|_{\dot{CAS}=0}})\sin\gamma_g, \gamma = \gamma_g]$
Constant altitude (ALT)	Constant CAS (CAS)	$\mathbf{p}_k = [VS = 0, e = k\|_{\dot{CAS}=0}]$	$\mathbf{u}_{k-1} = [T = D(\mathbf{x}), \gamma = 0]$

either, since these are not typically used in a descent and approach procedure.

III. SYSTEM MODEL AND FILTERING STRATEGY

A. System Model

In general, the nonlinear discrete state-space model (SSM) of interest is defined by the following process and measurement equations pair,

$$\begin{aligned} \mathbf{x}_k &= \mathbf{f}_{k-1}(\mathbf{x}_{k-1}, \mathbf{u}_{k-1}, \mathbf{p}_k) + \mathbf{q}_{k-1} \\ \mathbf{y}_k &= \mathbf{h}_k(\mathbf{x}_k, \mathbf{p}_k) + \mathbf{r}_k \end{aligned} \tag{1}$$

with k referring to the discrete time instants, $\mathbf{x}_k$ the states of the system, $\mathbf{y}_k$ the observation vector, and where $\mathbf{f}_{k-1}(\cdot)$ and $\mathbf{h}_k(\cdot)$ are the known system model functions (process and measurement, respectively). Both process and observations are corrupted by additive zero-mean Gaussian noise, $\mathbf{q}_{k-1} \sim \mathcal{N}(0; \mathbf{Q}_{k-1})$ and $\mathbf{r}_k \sim \mathcal{N}(0; \mathbf{R}_k)$ with covariance matrices $\mathbf{Q}_{k-1}$ and $\mathbf{R}_k$, typically assumed to be known. $\mathbf{u}_{k-1}$ is a control input, and $\mathbf{p}_k$ a vector of input parameters.

Regarding the data sources of the observation vector, the combination of ADS-B and Enhanced Mode-S Surveillance (EHS) are used in this paper. Indeed, the Enhanced Mode-S Surveillance (EHS) technology is designed as a dependent protocol by secondary surveillance radar to provide some flight parameters (such as the true airspeed, indicated airspeed, Mach number, and true heading of the aircraft) to improve all sorts of ATC systems. Besides, ADS-B is a newer data source using an automatically broadcasting technology and independent protocol that allows aircraft to send the identification, position, speed, and other flight parameters (such as vertical speed), which come from the on-board air data and navigation systems [10].

Taking into account the application at hand, and disregarding the time dependence for simplicity, at every time step:

- The state to be inferred is $\mathbf{x} = [h_p, v, m, \tau, p]^\top$: h_p the pressure altitude, v the true airspeed (TAS), m the mass of the aircraft, τ the temperature and p the air pressure.
- The measurements available from ADS-B and EHS are given by $\mathbf{y} = [h_p, v, \dot{h}, VS, CAS, M]^\top$: h_p the pressure altitude, v the TAS, $\dot{h}$ the derivative of the geometric altitude, VS the vertical speed which represents the rate of change of the pressure altitude [1], CAS the Calibrated AirSpeed, and M the Mach number.
- The control vector is given by $\mathbf{u} = [T, \gamma]^\top$, with T the engine thrust and γ the aerodynamic FPA.
- Since the pilot uses two independent actuators to steer the aircraft along the vertical plane, the so-called pilot input parameters vector $\mathbf{p}$ is composed of two parameters: the first parameter corresponds to the throttle setting and the second one is associated to the elevator. Such parameters must be taken into account to describe the specific guidance mode nonlinear dynamic system (refer to [7] for details).

In the application at hand, it is reasonable to consider process noise only on temperature and pressure, $\mathbf{q} = [\mathbf{0}_{1*3}, w_\tau, w_p]^\top$, with w_τ and w_p statistically independent, and their corresponding variances set according to the expected deviation from the standard atmospheric conditions. It is worth noting that the initial system state $\mathbf{x}_0$ can be obtained from flight and weather data, except for the mass of the aircraft which is unknown (we assume that it is not expected to be shared by the airlines, although, airlines are able to deliver it depending on their policy and the confidentiality of data), typically set to the 90% of the maximum landing mass.

The previous definitions provide the overview of the estimation problem of interest, that is, at every k infer $\mathbf{x}_k$ using observations up to time k, $\mathbf{y}_{1:k}$, but nothing has been said yet about the process and measurement functions.

Regarding the aircraft dynamic model (related to $\mathbf{f}_{k-1}(\cdot)$), few applications use basic kinematics that directly model the path characteristics of the aircraft. In contrast, FMS and accurate ground-based trajectory predictors use the well-known aircraft point-mass model: a three degrees of freedom (3DoF) model that assumes aircraft stability (i.e., rotational dynamics is not modelled) and therefore, only the aerodynamic, propulsive, and external forces (e.g., due to the gravity) are taken into account. This model is considered accurate enough for all ground-based air traffic management applications [11]. A further simplification of the 3DoF point-mass model leads to the so-called *gamma-command model*, where continuous vertical equilibrium is assumed, being the model considered in this contribution. In this case, the motion of the aircraft in

[1] In ISA condition, $h_p = h$, and consequently $VS = \dot{h}$

a vertical plane can be described by the following system of ordinary differential equations (ODEs),

$$\begin{aligned}\frac{dh}{dt} &= \dot{h} = v\sin\gamma \\ \frac{dv}{dt} &= \dot{v} = \frac{T-D}{m} - g\sin\gamma \\ \frac{dm}{dt} &= \dot{m} = -FF \\ \frac{d\tau}{dt} &= \dot{\tau} = \tau_h(h)\frac{dh}{dt} \\ \frac{dp}{dt} &= \dot{p} = p_h(\tau,p)\frac{dh}{dt}\end{aligned} \tag{2}$$

where $\tau_h(h)$ is the temperature partial derivative with respect to the geometric altitude, and it is set to a constant value according to the international standard atmosphere (ISA) temperature lapse rate. In hydrostatic equilibrium $p_h(\tau,p) = -\rho g$ is the pressure partial derivative with respect to the geometric altitude, with g the gravity acceleration and $\rho = \frac{p}{R\tau}$ the density of the air, where $R = 287.053\,\text{J/kg K}$ the air perfect gas constant. D is the aerodynamic drag and FF is the engine fuel flow.

To further complete the previous equations, we can write the pressure altitude as a function of the geometric altitude as,

$$h_p(h) = \begin{cases} \frac{\tau_{SSL}}{\lambda_\tau}\left(1 - \left(\frac{p}{P_{Ref}}\right)^{\frac{R\lambda_\tau}{g}}\right) & \text{if } h \le h_{tropo} \\ h_{tropo} - \frac{R\tau_{11}}{g}\ln\frac{p}{P_{11}} & \text{if } h > h_{tropo} \end{cases} \tag{3}$$

with $h_{tropo} = 11.000\,\text{m}$, $\tau_{SSL} = 288.15\,\text{K}$ the standard sea level air temperature, $\lambda_\tau = 0.0065\,\text{K/m}$ the temperature gradient, P_{Ref} the reference pressure associated with the transition level, $\tau_{11} = 216.65\,\text{K}$, $p_{11} = 22632\,\text{Pa}$. Under the ISA condition, assumed in this paper, the pressure altitude is equal to the geometric altitude, therefore providing the link between the first ODE equation and the first state variable h_p.

As clearly explained in [7], in order to integrate (2) we must close two degrees of freedom, linked to the pilot throttle and elevator. Indeed, such pilot inputs could directly control the thrust T and FPA γ, but aircraft are not operated following specific T and γ profiles, and instead are composed of different guidance mode segments (i.e., constant Mach or CAS segments for climbs and descents). Therefore, two path constraints are needed (refer to [7] for details). The pilot (or FMS) input parameter vector is given by $\mathbf{p} = [\pi, VS, \gamma_g, e]^\top$: π the throttle, γ_g the ground FPA, VS the vertical speed and e the energy share factor. In general, we define three different energy share factors according to the guidance mode: i) the energy share factor in the direct input fixed to a known value; ii) the aircraft is flying at constant CAS, resulting to an energy share factor as function of atmospheric parameters; and iii) similar as previous case, the aircraft is flying at constant Mach. Each guidance mode is defined by a combination of two path constraints, which depend on two of the parameters in $\mathbf{p}$. In other words, two of the pilot inputs are used in each guidance mode to compute the input vector $\mathbf{u}$ and obtain $\mathbf{f}_{k-1}(\cdot)$. Notice that the measurement function $\mathbf{h}_k(\cdot)$ can be directly expressed from $\mathbf{x}_k$ and $\mathbf{p}_k$.

B. An Interacting Multiple Model Filtering Approach

For linear SSMs the best linear filter which minimizes the mean square error (MSE) is the Kalman filter (KF) regardless of the noise distribution, provided that we have a perfect knowledge of the system: known system matrices, known noise mean and covariance, known inputs and perfect initialization. For nonlinear SSMs, the most popular solution is the extended KF (EKF), which uses a first order approximation of the nonlinear system model and the standard linear KF solution [12]. These filters apply for a single dynamics SSM, but as previously stated, in the problem of interest we have several guidance modes which lead to a set of different dynamic models. A possible solution to cope with such problem formulation is to resort to the so-called Interacting Multiple Model (IMM) filter [13], [14], where several (interconnected) filters run in parallel, each one matched to a specific SSM. If the system is nonlinear, as considered in this contribution, this implies to use a bank of EKFs, denoted EKF-IMM. In this paper, the generic EKF-IMM algorithm (refer to [13], [14] for the formulation details) has been adapted to identify the exact flap deployment moment. In order to accomplish that, different models have been defined, each one corresponding to a given configuration setting and a specific guidance mode, where two parameters are controlled. The different modes are shown in Table I. Notice that the output of the EKF-IMM provides both an estimate of the state vector and the model probability associated to each of the guidance modes. The latter can be directly used for real-time flap deployment identification.

Moreover, notice that the transition matrix which specifies the probabilities of switching from one guidance mode to another is given by: $P(j|i) = P_{i,j} = 0.02$ for $i \neq j$ and $P_{i,j} = 0.98$ for $i = j$.

IV. Results and Discussion

This section displays and discusses the results obtained for a set of representative aircraft descent profiles, which are generated via a custom trajectory simulator considering an Airbus A320 aircraft. First, details on the validation trajectories (VT) are given in Section IV-A, and the simulation results are shown and discussed in Section IV-B.

A. Simulation Setup

The trajectory simulator generates flight data which contains the same information that could be obtained from ADS-B and a selective mode transponder (Mode S) receiver. The trajectories are divided into several flight phases, each one expressed in terms of a parametrised guidance mode being targeted and an end condition to be met. The initial condition of the trajectories profile can be described as the initial mass of the aircraft, the pressure altitude, the speed and the geometric position. The profile starts at the initial condition and the trajectory is numerically integrated according to the guidance mode until reaching the end condition. In turn, this end condition is used as the initial condition for the next trajectory phase [7]. Thus, the starting time of each phase is the ending time of the previous one. The simulator is

TABLE II. VERTICAL PROFILE SPECIFICATION OF THE VALIDATION TRAJECTORY (VT1)

Phase	Guidance Mode	Mode1	Mode2	End Condition	Configuration	Landing Gear
1	THR-CAS	Idle	250 kt	$h_p = 4000$ ft	CLEAN	UP
2	THR-DEC	Idle	0.3	$CAS = 193$ kt	CLEAN	UP
3	VS-CAS	-500 ft/min	193 kt	$\Delta s = 2$ NM	CONF 1	UP
4	FPA-DEC	$-3°$	0.76	$h_p = 2000$ ft	CONF 1	UP
5	FPA-DEC	$-3°$	0.6835	$h_p = 1500$ ft	CONF 2	UP
6	FPA-DEC	$-3°$	0.53	$CAS = 147$ kt	CONF 3	DOWN
7	FPA-DEC	$-3°$	0.472	$CAS = 128$ kt	FULL	DOWN
8	FPA-CAS	$-3°$	128 kt	$h_p = 50$ ft	FULL	DOWN

TABLE III. VERTICAL PROFILE SPECIFICATIONS OF THE VALIDATION TRAJECTORIES (VT2,VT3,VT4,VT5)

Phase	Guidance Mode	Mode1	Mode2	End Condition	Flap position	LG
1	THR-CAS	Idle	250 kt	$h_p = 4000$ ft	CLEAN	UP
2	THR-DEC	Idle	0.3	$CAS = v2$	CLEAN	UP
3	THR-DEC	Idle	0.3	$CAS = 193$ kt	CONF 1	UP
4	VS-CAS	-500 ft/min	193 kt	$\Delta s = 2$ NM	CONF 1	UP
5	FPA-DEC	$-3°$	0.76	$h_p = 2000$ ft	CONF 1	UP
6	FPA-DEC	$-3°$	0.6835	$h_p = 1500$ ft	CONF 2	UP
7	FPA-DEC	$-3°$	0.53	$CAS = 147$ kt	CONF 3	DOWN
8	FPA-DEC	$-3°$	0.472	$CAS = 128$ kt	FULL	DOWN
9	FPA-CAS	$-3°$	128 kt	$h_p = 50$ ft	FULL	DOWN

TABLE IV. VERTICAL PROFILE SPECIFICATION OF THE VALIDATION TRAJECTORIES (VT6,VT7,VT8)

Phase	Guidance Mode	Mode1	Mode2	End Condition	Flap position	LG
1	THR-CAS	Idle	250 kt	$h_p = 4000$ ft	CLEAN	UP
2	THR-DEC	Idle	0.3	$CAS = 193$ kt	CLEAN	UP
3	VS-CAS	-500 ft/min	193 kt	$\Delta s = s3$	CLEAN	UP
4	VS-CAS	-500 ft/min	193 kt	$\Delta s = s4$	CONF 1	UP
5	FPA-DEC	$-3°$	0.76	$h_p = 2000$ ft	CONF 1	UP
6	FPA-DEC	$-3°$	0.6835	$h_p = 1500$ ft	CONF 2	UP
7	FPA-DEC	$-3°$	0.53	$CAS = 147$ kt	CONF 3	DOWN
8	FPA-DEC	$-3°$	0.472	$CAS = 128$ kt	FULL	DOWN
9	FPA-CAS	$-3°$	128 kt	$h_p = 50$ ft	FULL	DOWN

TABLE V. END CONDITION PARAMETRISATIONS

	VT2	VT3	VT4	VT5	VT6	VT7	VT8
$v2$	230 kt	210 kt	220 kt	200 kt			
s3					0.5 NM	0.75 NM	1 NM
s4					1.5 NM	1.25 NM	1 NM

based on Eurocontrol's Base of Aircraft Data (BADA) aircraft performance models [15].

Table II gives details on the typical descending profile for the first validation trajectory (VT1), including the corresponding guidance modes and their associated values, the end condition, the flap position, and the landing gear position. In this VT, the pilot decides to start using flaps at phase 3, and simultaneously switches from flying with idle thrust and deceleration to constant VS and constant CAS.

Table III gives the typical profiles associated to VT 2 to 5, where the flaps are deployed without changing the guidance mode. In this case the flaps are deployed while flying in idle thrust and deceleration mode. The difference among VT 2 to 5 is the end condition of the second phase (i.e., CAS = $v2$, with the corresponding values summarised in Table V).

Table IV concerns the last three typical VT profiles (VT 6 to 8), for which the flaps are deployed while flying at constant VS and constant CAS, at three different moments (refer to the end condition $\Delta s = s3$ and $\Delta s = s4$ in Table IV, and the corresponding values summarised in Table V).

Figure 1 illustrates the geometric altitude, true airspeed, and CAS for the descending profiles associated to VT4 and VT7, as an example of the 8 VT. The vertical pink lines show the start time of each phase of the profile, and the vertical black line indicates the flap deployment moment.

B. Results

In the simulations we consider the general nonlinear discrete SSMs in Section III, taking into account that the measurement noise is a zero-mean Gaussian with known covariance $\mathbf{R} = \text{diag}((5\,\text{ft})^2, (5\,\text{kt})^2, (25\,\text{ft/min})^2, (25\,\text{ft/min})^2, (5\,\text{kt})^2, 10^{-3})$. Recall that one of the outputs of the EKF-IMM is the model probability, which is exploited in this contribution for flap deployment identification. For each VT we perform 1000 Monte Carlo runs in order to obtain statistically meaningful results. The average model probability around the flap deployment moment (two phases at the vicinity of the flap deployment moment), for the different VT, is shown in Figure

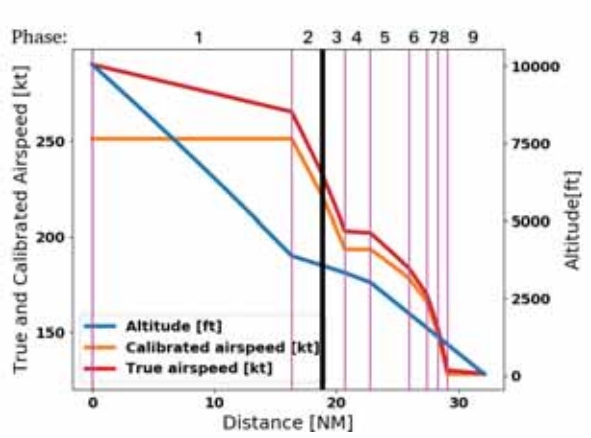

(a) VT4

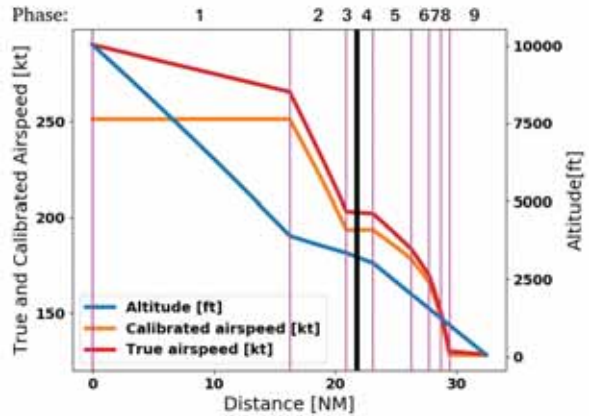

(b) VT7

Figure 1. Descending profiles for VT4 and VT7. Start of the different phases indicated with the pink vertical lines, and flap deployment illustrated by the vertical black line.

2. Indeed, results Figure 2 focus on the flap deployment moment, but the whole trajectory is estimated. For each VT, the upper subplot shows the real guidance mode, and the lower subplot the average estimated mode probability. It is easy to see that in most of the cases the EKF-IMM is able to estimate the correct guidance mode (i.e., taking the model with maximum probability among the pool of possible modes).

Figure 2 also shows the average estimated flap deployment moment (vertical black dashed line). Notice that in order to avoid false alarms, or equivalently, to increase the method's robustness, this value is computed using a moving average of the EKF-IMM outcome mode probabilities, with a window size equal to $N = 5$ samples. Obviously, there exists a performance versus robustness trade-off which requires a dedicated study (i.e., w.r.t. the window size, the flap deployment moment, the system parameters, etc.) and is left for future work.

The moving average method implicitly induces a method response delay, that is why in subplots (a) to (e) in Figure 2 there is a slight shift to the right w.r.t. the true flap deployment time instant. Indeed, this is not only because of the moving average but also because the EKF-IMM also needs a short time lapse to adapt to the new mode when switching between two different configuration settings. It is interesting to notice that in the last three VT, that is, VT6 to VT8, the IMM is not able to correctly decouple the identification of VS-CAS clean mode from the VS-CAS CONF1 mode. This has a direct impact on the results, and the high-lift device deployment moment estimate appears before the real mode change.

To further complete the previous results a box-and-whiskers plot is shown in Figure 3 to be able to better understand the flap deployment moment estimation error (in seconds in the plot) for all VTs. For each VT, the bottom and top of the box represent the first and third quartiles, respectively. The lines extending vertically from the boxes (whiskers) indicate the variability outside these quartiles, while the ends of the whiskers represent the 1.5 interquartile range of the first and third quartile. Finally, the red line inside the box is provides the median, and outliers are represented in red points.

It is interesting to acknowledge again a significantly different IMM behaviour depending on the descent configuration. Indeed, because of the moving average procedure using $N = 5$ samples, one would expect the average estimation error to be between 0 and -5 seconds, which is the case for VT2, VT4 and VT5, but the error slightly increases for VT1 and VT3, meaning that the IMM takes some extra time to respond to the mode change. As already stated, because the IMM is not able to correctly decouple the VS-CAS clean mode from the VS-CAS CONF1 mode, then the error is positive for VT6 to VT8. In any case, the average method performance is good enough to validate the proposed methodology.

In this paper, the metric to measure the filter performance is the difference between the real and estimated deployment time, in seconds. If we take the true airspeed of the aircraft at the moment CONF 1 is deployed, the error in distance is always below 1 NM. These are promising results, taking into account the performance of similar studies found in the literature, such as [4]. We have to keep in mind, however, that in this paper the validation has been done with a few number of simulated trajectories.

V. Conclusion

In this contribution, an IMM filtering approach has been proposed for real-time identification of the high-lift device deployment moment in aircraft descents. The underlying idea was to exploit the fact that aircraft fly following different guidance modes (each one related to a specific dynamic model), reason why a multiple model filtering strategy must be accounted for, and study if such multiple model filter was able to identify the difference between clean and deployed high-lift configurations. Instead of using the standard state estimate outcome of the IMM, the model probabilities were used to determine the high-lift deployment moment. In addition, to avoid false alarms and further improve the robustness of the proposed method, a moving average was applied to such IMM model probabilities. A custom trajectory simulator was used to release high rate data ($1\,s$). Without entering into the method's

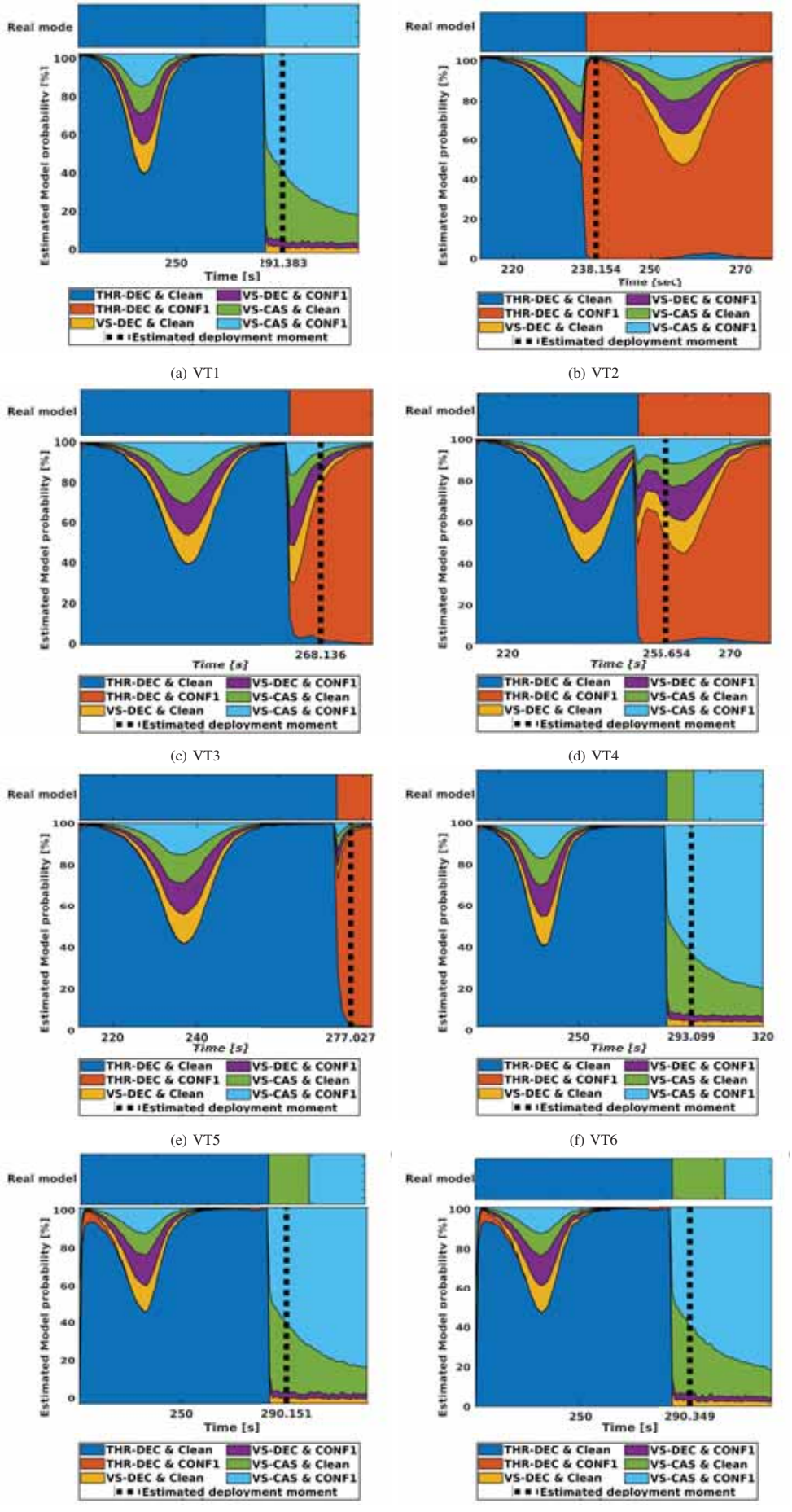

(a) VT1 (b) VT2

(c) VT3 (d) VT4

(e) VT5 (f) VT6

(g) VT7 (h) VT8

Figure 2. Considering the trajectory region around the flap deployment moment, each subplot provides, for each validation trajectory (VT): 1) the real guidance mode, 2) average estimated model probability, and 3) the estimated flap deployment moment.

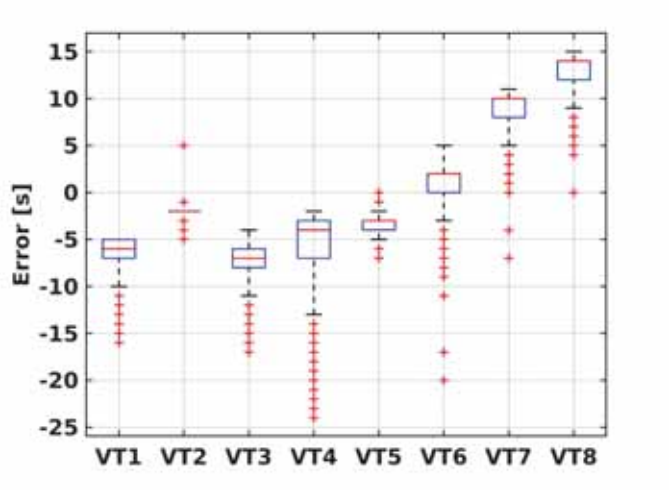

Figure 3. Estimation error of flap deployment moment

computational complexity details, it is worth pointing out that the filter running time is low enough to ensure a real-time implementation. The preliminary results in this article show the good performance of the IMM-based high-lift deployment identification, being a promising solution for such application.

Accurate and reliable trajectory prediction is fundamental for the design of next generation air traffic services (ATS), decision support tools for traffic synchronization and separation management; as well as enhanced safety nets and collision avoidance tools; either in a (partially) automated environment, on-ground, airborne or in a distributed system. This contribution could help to develop future ground-based monitoring tools, aiming at detecting atypical trajectories and/or preventing unstabilised approaches, but could enable as well advanced trajectory prediction capabilities benefiting many ATM applications.

Several points must be addressed in future work : i) use historical data gathered from ADS-B receivers to assess the method performance with real data; ii) extend the method to other configuration settings containing different flap positions, and landing gear up/down; iii) analyse the impact of real-time flap deployment identification on ground-based tools; and iv) consider atypical trajectories and other types of aircraft.

REFERENCES

[1] G. Jarry, D. Delahaye, F. Nicol, and E. Féron, "Aircraft atypical approach detection using functional principal component analysis," *Journal of Air Transport Management*, vol. 84, May 2020.

[2] F. Jackman, "Nearly half of commercial jet accidents occur during final approach, landing," *AeroSafety world*, vol. 9, 2014.

[3] FSF ALAR task force, "Stabilized approach," Flight Safety Foundation (FSF), Alexandria, VA, Tech. Rep., 2000, approach and landing accident reduction (ALAR) - briefing note 7.1.

[4] G. Jarry, D. Delahaye, and E. Feron, "Approach and landing aircraft on-board parameters estimation with lstm networks," in *2020 International Conference on Artificial Intelligence and Data Analytics for Air Transportation (AIDA-AT)*. IEEE, 2020, pp. 1–6.

[5] J. Sun, J. Ellerbroek, and J. M. Hoekstra, "Aircraft initial mass estimation using bayesian inference method," *Transportation Research Part C: Emerging Technologies*, vol. 90, pp. 59–73, 2018.

[6] R. Dalmau, X. Prats, A. Ramonjoan, and S. Soley, "Estimating fuel consumption from radar tracks: A validation exercise using FDR data from descent trajectories," in *Proceedings of the 8th International Congress on Research in Air Transportation (ICRAT)*. Castelldefels, Catalonia: Eurocontrol/FAA, Jun 2018.

[7] R. Dalmau, M. Pérez-Batlle, and X. Prats, "Real-time Identification of Guidance Modes in Aircraft Descents Using Surveillace Data," in *Proc. of the IEEE/AIAA Digital Avionics Systems Conference*, 2018.

[8] M. Soler, *Fundamentals of Aerospace Engineering: An introductory course to aeronautical engineering*. Manuel Soler, 2014.

[9] J. Bronsvoort, "Contributions to Trajectory Prediction Theory and its Application to Arrival Management for Air Traffic Control," Ph.D. dissertation, Technical University of Madrid (UPM), Madrid, Spain, 2014.

[10] J. Sun, "Open Aircraft Performance Modeling: Based on an Analysis of Aircraft Surveillance Data." Ph.D. dissertation, Delft University of Technology (TUDelft), Delft, Netherlands, 2019.

[11] R. Dalmau, "Optimal Trajectory Management for Aircraft Descent Operations Subject to Time Constraints." Ph.D. dissertation, Technical University of Catalonia (UPC), Barcelona, Spain, 2019.

[12] B. Anderson and J. B. Moore, *Optimal filtering*. Englewood Cliffs, NJ: Prentice–Hall, 1979.

[13] H. A. Blom and Y. Bar-Shalom, "The interacting multiple model algorithm for systems with markovian switching coefficients," *IEEE transactions on Automatic Control*, vol. 33, no. 8, pp. 780–783, 1988.

[14] X. R. Li and V. P. Jilkov, "Survey of Maneuvering Target Tracking. Part V: Multiple-Model Methods," pp. 1255–1321, Oct. 2005.

[15] Eurocontrol, "User manual for the base of aircraft data (BADA). revision 4.1," Eurocontrol, Bretigny, France, Tech. Rep., 2014.